Applied Catalysis B: Environmental 115–116 (2012) 336–345

Contents lists available at SciVerse ScienceDirect

Applied Catalysis B: Environmental

journal homepage: www.elsevier.com/locate/apcatb

Efficiency and reactivity pattern of ceria-based noble metal and transition metal-oxide catalysts in the wet air oxidation of phenol

Francesco Arena[a,b,*], Cristina Italiano[a], Lorenzo Spadaro[a,b]

[a] Dipartimento di Chimica Industriale e Ingegneria dei Materiali, Università degli Studi di Messina, Viale F. Stagno D'Alcontres 31, I-98166 Messina, Italy
[b] Istituto CNR-ITAE "Nicola Giordano", Salita S. Lucia 5, I-98126 S. Lucia Messina, Italy

ARTICLE INFO

Article history:
Received 16 November 2011
Received in revised form
19 December 2011
Accepted 22 December 2011
Available online 31 December 2011

Keywords:
Catalytic wet air oxidation (CWAO)
Phenol
Transition-metal oxide catalysts
Noble-metal catalysts
Activity
Selectivity
Stability
Reaction mechanism
Kinetics

ABSTRACT

The activity-stability pattern of ceria-based noble metal (Pt/CeO_2) and transition metal-oxide ($MnCeO_x$) catalysts in the wet air oxidation of phenol (CWAO) at different catalyst-to-phenol weight ratio (*R*, 1–5) was comparatively probed using a stirred batch reactor with continuous oxygen feed (T_R, 150 °C; P_{O_2}, 0.9 MPa). Both Pt/CeO_2 and $MnCeO_x$ systems drive a surface *dual-site* Langmuir–Hinshelwood (L–H) reaction path enabling higher efficiency, different reaction kinetics and "phenol-total organic carbon" conversion relationships in comparison to homogeneous CWAO catalysts [1]. A simplified reaction scheme based on consecutive *adsorption* and *mineralization* steps and the relative kinetic analysis show that the former determines the rate of phenol and TOC removal, while the latter controls the selectivity and rate of catalyst fouling. The $MnCeO_x$ system ensures a fast and complete phenol conversion and a TOC removal higher than 80% at any *R*, while improved adsorption and mineralization functionalities explain a higher resistance to deactivation by fouling than Pt/CeO_2 system.

1. Introduction

The extraordinary industrial development of the last decades is at the origin of the constantly rising concern on process-waters recycle and disposal of harmfully polluted wastewaters [2–7]. Also urged by even more stringent environmental regulations, this is pressing a big interest on novel technologies alternative or complementary to biological treatments for attaining an efficient detoxification of various industrial (oil, chemical, pharmaceutical, polymers, agro-food, electronics, dyes, etc.) aqueous streams containing high loads of organic pollutants, characterized by low biodegradability and high toxicity [2–9]. To date available technologies accomplish a liquid-phase oxidative mineralization of noxious pollutants using costly oxidants (H_2O_2, $KMnO_4$, O_3, UV/γ-irradiation, etc.) in small-scale (low COD load and feed rate) *advanced oxidation* (AOP) [2,3,6–9] or oxygen/air in the presence of suitable catalysts in so called *catalytic wet air oxidation* (CWAO) processes [1–6,8–30]. Despite superior efficiency, versatility and cost-effectiveness for large-scale applications, however the discovery of cheap, robust and active catalyst(s) still represents the main challenge of the heterogeneous CWAO technology [2–6,8,9]. In fact, combining a high decontamination efficiency with an adequate resistance to *leaching* [3–5,8,10–14,18–20] and *fouling* [10–14,19] phenomena, $MnCeO_x$ composite systems currently represent the most promising alternative to noble-metal catalysts, generally used in still rare worldwide processes [2–6,8,9]. However, lack of systematic data on "catalyst–substrate" systems and different testing conditions and/or reactor configurations have impeded a definitive assessment of the CWAO mechanisms and kinetics for decisive catalyst improvements [1,8–31]. In fact, beside to the specific chemistry of the catalyst–substrate system, inter-phase mass transfer phenomena determine mechanism and kinetics of the CWAO process by affecting the transport rate of substrate and oxygen to the catalyst surface [3,5,6,9]. Then, even if the CWAO of phenol is usually described by a *free-radical* reaction model [3–5,8–10,15,19–28,30,31], many authors relate the

Abbreviations: *R*, catalyst-to-phenol weight ratio; k_{Ph}, pseudo 1st-order kinetic constant of phenol concentration decay (h^{-1}); k_{CO_2}, pseudo 1st-order kinetic constant of CO_2 formation (h^{-1}); $rate_{Ph}$, rate of phenol concentration decay ($mol\,L^{-1}\,h^{-1}$); k_{ads}, pseudo 1st-order catalytic constant of phenol adsorption ($k_{ads} = k_{Ph}/C_{cat}$, $L\,g_{cat}^{-1}\,h^{-1}$); k_{ox}, pseudo 1st-order catalytic constant of phenol oxidation ($k_{ox} = k_{CO_2}/C_{cat}$, $L\,g_{cat}^{-1}\,h^{-1}$); SSA_{ads}, specific surface rate of phenol adsorption ($mol\,m_{cat}^{-2}\,h^{-1}$); SAC, surface adsorption capacity ($g_{Ph}\,m_{cat}^{-2}$).

* Corresponding author.
E-mail address: Francesco.Arena@unime.it (F. Arena).

0926-3373/$ – see front matter © 2011 Elsevier B.V. All rights reserved.
doi:10.1016/j.apcatb.2011.12.035

superior water detoxification performance of $MnCeO_x$ systems to the occurrence of a classic Langmuir–Hinshelwood (L–H) surface path [1,3,9,11–14,18–22,29].

Therefore, this paper is aimed at providing a comparative assessment of the activity and stability patterns of ceria-supported noble metal (Pt/CeO_2) and transition metal-oxide ($MnCeO_x$) catalysts in the CWAO of phenol. The occurrence of a *dual-site* Langmuir–Hinshelwood (L–H) reaction path explains different phenol-TOC conversion relationships in comparison to the homogeneous process, while a simple reaction network based on adsorption and mineralization steps and the relative kinetic analysis provide evidence of the main CWAO catalyst requirements.

2. Experimental

2.1. Materials

The $MnCeO_x$ (Mn_{at}/Ce_{at}, 1.5) system was prepared via the co-precipitation route according to the procedure elsewhere described [1,13,14], while a 5 wt% Pt/CeO_2 (Pt_{at}/Ce_{at}, 0.05) catalysts was obtained by incipient wetness impregnation of a high surface area "lab-made" ceria sample [32] with a $Pt(NH_3)_4(NO_3)_2$ solution (pH ≈ 6) and subsequent drying at 90 °C [28]. Before testing the catalyst was reduced in flowing hydrogen (0.1 STP L/min) at 350 °C for 3 h, then flushed in a He flow and further passivated at r.t. under a 5% O_2/He mixture flow [28]. Metal dispersion ($D(\%) = 112/d_{VA}(nm)$) was probed by TEM observations (not reported for the sake of brevity) and a statistical estimate of the mean volume–area (d_{VA}) particle size:

$$d_{VA} = \frac{\sum_i n_i d_i^3}{\sum_i n_i d_i^2} \approx 7\,\text{nm} \quad (1)$$

resulting equal to ca. 16% and corresponding to a metal surface area (MSA) of ca. 2 m^2_{Pt}/g_{cat}. The other main physico-chemical properties of the catalysts are given in Table 1.

3. Methods

Catalyst testing in the wet air oxidation of phenol at 150 °C and a total pressure of 1.4 MPa (P_{O_2}, 0.9 MPa) was carried out using a PTF-lined autoclave (0.25 L) equipped with a magnetically driven turbine impeller (≈800 rpm). The reactor was loaded with 140 mL of distilled water and catalyst samples of 0.15, 0.30 and 0.75 g, corresponding to catalyst-to-phenol weight ratio (R) of 1, 2 and 5 respectively, and fed with a continuous oxygen flow at the rate of 0.1 STP L/min. After heating to reaction temperature (150 °C), a 10 mL aqueous solution of phenol, corresponding to a concentration of 1.0 ± 0.05 g/L in the cumulative volume of 150 mL, was introduced into reactor by a pressurized injection system located on the reactor head. This is the initial reaction time (t_0) at which the (initial) phenol concentration is formally taken equal to 1 g/L. Under the adopted conditions, the calculated Weisz–Prater number (N_{W-P}) for finely powdered ($d_p \leq 10\,\mu m$) catalyst samples and phenol 1st-order reaction kinetics

$$N_{W-P} = \frac{r_{app}\rho_p(d_p/2)^2}{D_{eff}C_{phen,S}} < 0.15 \quad (2)$$

is always lower than 0.008 (see Fig. A of Supplementary information), confirming the lack of diffusional resistances on the reaction kinetics. The kinetic regime of the catalyst testing was further experimentally verified by the analogous activity–selectivity pattern found for the more active $MnCeO_x$ catalyst, using fivefold concentrations of both phenol (5 g/L) and catalyst (25 g/L) at $R = 5$ (Fig. A of Supplementary Information).

The reaction was monitored by withdrawing ca. 1 mL reaction solution samples that were analyzed with respect to pH, phenol and intermediates and total organic carbon (TOC) concentration. Namely, phenol and intermediates were detected by a HPLC (UVD17OU, DIONEX) equipped with a C6-Phenyl 110A column and a dual-channel UV–vis detector set at 210 nm, using a buffered (pH = 2.5) 3% methanol aqueous solution as mobile phase (0.8–2 mL min^{-1}). The identification of the various intermediates and the calibration of the detector were made using reference compounds solutions. The TOC content was determined by a TOC combustion-nondispersive IR analyzer (TOC-VCSN, Shimadzu).

Volatile organic compounds stripped away from the reactor were trapped by bubbling the outlet gaseous flow in a cold (4 °C) water trap (≈10 mL), which was analyzed by HPLC and TOC measurements [1]. In addition, the CO_2 selectivity was probed by gravimetric analyses of the precipitated $BaCO_3$ formed by further bubbling the stream from the cold trap into a saturated $Ba(OH)_2$ solution kept under stirring at r.t. [1,13,14,16,17,29].

The reproducibility of catalytic data with reference to phenol and TOC conversion, CO_2 selectivity and pH was better than 90%.

Thermogravimetric (TGA-DSC) analysis of the "used" Pt/CeO_x and $MnCeO_x$ catalysts was performed using a Simultaneous Thermal Analysis Instrument (STA 409C, NETZSCH) operating in air with a heating rate of 10 °C/min. Used catalysts were recovered from the reaction solution by filtration, washed with distilled water and further dried in air at 100 °C.

X-ray photoelectron spectroscopy (XPS) analysis of the fresh and used catalysts was performed by a XPS spectrometer (Physical Electronics GMBH PHI 5800-01) using a monochromatized Al Kα radiation with a power beam of 250 W and a pass energy of 58.70 eV. The studied BE ranges were 280–300 eV (C_{1s}), 524–540 eV (O_{1s}), 62–86 eV (Pt_{4f}), 635–680 eV (Mn_{2p}), and 870–935 eV (Ce_{3d}). Signals calibration for the fresh samples was done with reference to the C_{1s} line of *adventitious carbon* (284.8 eV), while C forms (C, $CO_3^=$, C—H, etc.) on the used samples were referred to the Ce_{3d} u''' transition at 916.2 eV.

Surface reactive oxygen availability (SROA) measurements at 150 °C were carried out in a pulse mode using He as carrier gas. A catalyst sample of ca. 20 mg diluted with α-Al_2O_3 (1/10, w/w) was loaded into a quartz reactor and heated to 150 °C (10 °C/min) in a 20% O_2/He flow (30 STP mL min^{-1}). After an isotherm of 30 min, the reactor was switched in the carrier flow until stabilization of the baseline and then 0.66 STP mL pulses of a 20% CO/He mixture were injected until the end of CO consumption.

4. Results and discussion

4.1. Reactivity pattern of Pt/CeO_2 and $MnCeO_x$ catalysts

The CWAO behavior pattern of the Pt/CeO_2 (A, C, E) and $MnCeO_x$ (B, D, F) systems at catalyst-to-phenol ratio (R) of 5 (A and B), 2 (C and D) and 1 (E and F) is compared in Fig. 1 in terms of phenol and TOC conversion, pH and CO_2 selectivity *vs.* reaction time. In all the cases it is observable the lack of any induction time and an analogous *exponential-rising* trend of phenol conversion. In particular, the $MnCeO_x$ catalyst attains the 100% conversion at any R, while the Pt/CeO_2 system ensures the complete phenol conversion only at the highest R (5) and asymptotic final values of 55 and 40% for R of 2 and 1, respectively. The TOC conversion parallels that of phenol, though the $MnCeO_x$ system shows a decreasing trend after a maximum conversion coincident with full phenol conversion. The pH decreases always progressively to acidic values (Fig. 1), while the CO_2 selectivity of both catalysts increases regularly during reaction time until final values roughly proportional to R (Fig. 1).

Table 1
Physico-chemical properties of the catalysts.

Catalyst	Metal loading	Me_{at}/Ce_{at} (wt%)	SA_{BET} (m^2/g)	PV[a] (cm^3/g)	APD[b] (nm)	SROA[c] ($mmol_O/g_{cat}$)
Pt/CeO_2	5.1	0.05	89	0.26	27	0.568
$MnCeO_x$	26.5	1.40	84	0.32	22	0.166

[a] Pore volume.
[b] Average pore diameter.
[c] Surface reactive oxygen availability at 150 °C.

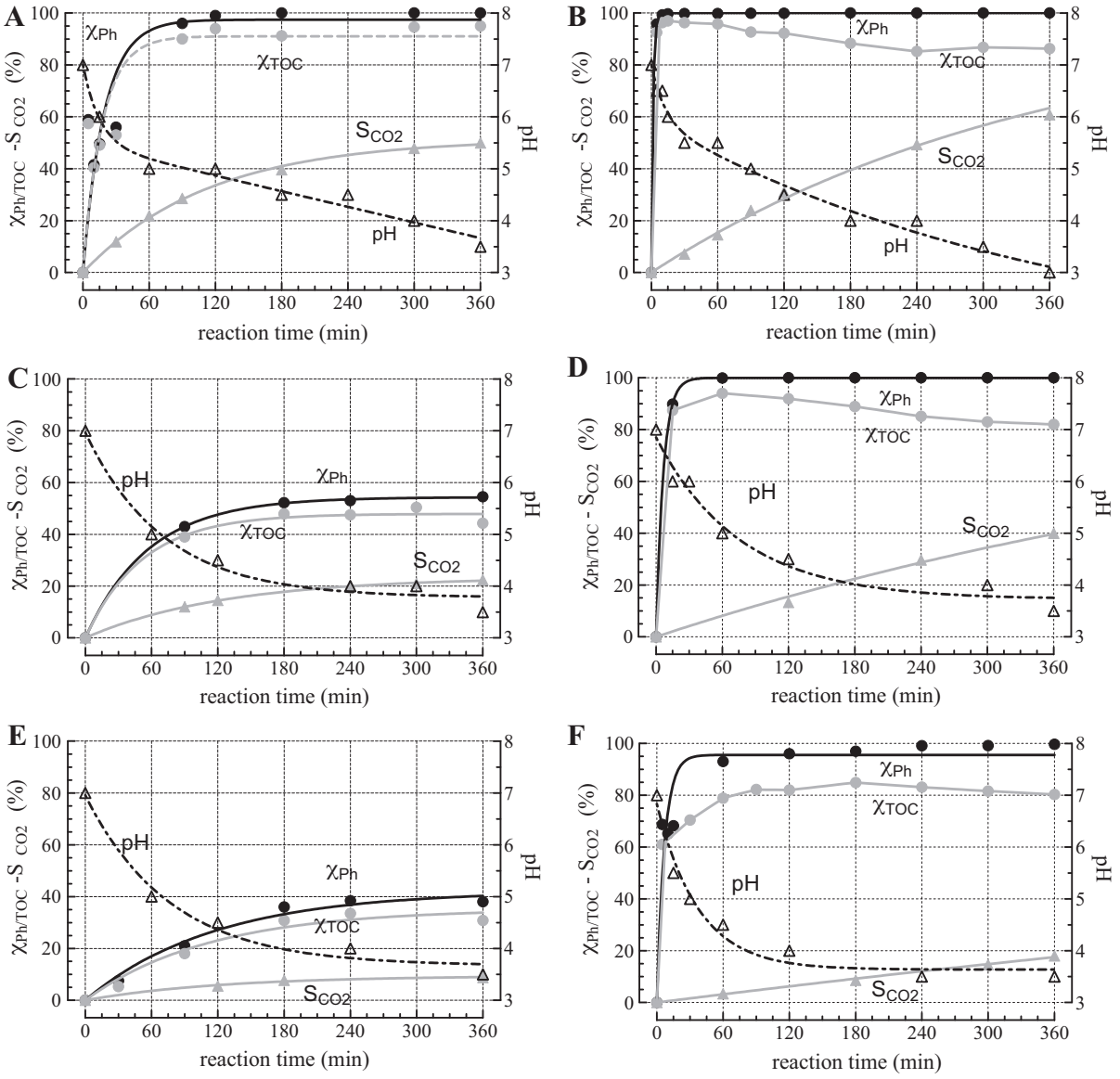

Fig. 1. CWAO pattern of phenol of heterogeneous Pt/CeO_2 (A, C, E) and $MnCeO_x$ (B, D, F) catalysts at 150 °C and catalyst-to-phenol weight ratio (R) of 5 (A and B), 2 (C and D) and 1 (E and F). Phenol (●) and TOC (○) conversion, pH (△) and CO_2 selectivity (▲) *vs.* reaction time.

Table 2
Final (t, 6 h) phenol and total organic carbon (TOC) conversion and CO_2 selectivity data, theoretic carbon content and TGA weight loss of the used catalysts.

Catalyst	R	$X_{Ph,fin}$ (%)	$X_{TOC,fin}$ (%)	$S_{CO_2,fin}$ (%)	Δ_{CMB}[a] (%)	V_{oc} (%)	C-content[b] (%)	ΔW_{TGA}[c] (%)
Pt/CeO_2	5	100	95	50	−45	–	−8	−6
	2	55	45	22	−23	10	−6	−5
	1	40	30	10	−20	13	−7	−6
$MnCeO_x$	5	100	85	60	−25	–	−5	−5
	2	100	80	40	−40	–	−17	−15
	1	100	80	20	−60	–	−38	−40

[a] Difference between $X_{TOC,fin}$ and S_{CO_2}.
[b] Theoretic carbon content of the used catalysts.
[c] Weight loss of the used catalysts recorded by TGA analysis.

In particular, at $R = 5$ the Pt/CeO_2 catalyst attains a complete phenol conversion in ca. 3 h, while the extent of TOC removal levels off to an asymptotic value of ca. 95%. According to raising concentrations of formic and, mostly, acetic acids (see Fig. B of Supplementary information) the pH decreases regularly to ca. 3.5, while the CO_2 selectivity attains a final value of 50% (Fig. 1A). With reference to the above TOC conversion (95%), the amount of CO_2 detected accounts for a gap in carbon mass-balance of ca. 45% (Table 2).

The superior CWAO efficiency of the $MnCeO_x$ catalyst is evident from the complete removal of both phenol and TOC in ca. 20 min (Fig. 1B). Afterward a slight and progressive rise of TOC (χ_{TOC}, 97 → 85%) signals the ongoing release (*desorption*) and accumulation of intermediate(s) during reaction time, mostly acetic acid (Fig. B of Supplementary information) responsible of the drop of pH to ca. 3.5 (Fig. 1B). Anyhow, a final CO_2 selectivity of 60% (Fig. 1B) accounts for a lack in carbon mass-balance of ca. 25% (Table 2).

For $R = 2$ the Pt/CeO_2 system shows an evidently lower efficiency, according to final phenol and TOC conversion values of ca. 55 and 45% respectively (Fig. 1C). The final CO_2 selectivity is ca. 20%, while the pH decreases progressively with a trend similar to that recorded in the previous run to 3.5. Also under such conditions the $MnCeO_x$ catalyst confirms its superior performance leading to a complete phenol removal after ca. 1 h (Fig. 1D). At this time the TOC abatement reaches a maximum of 90%, lowering afterwards to a final value of ca. 80% when a pH of 3.5 along with a CO_2 selectivity of ca. 40% are recorded (Fig. 1D). Under such conditions, the carbon mass balance signals a loss of ca. 25 and 40% for Pt/CeO_2 and $MnCeO_x$ catalysts, respectively (Table 2).

At least, for $R = 1$ the Pt/CeO_2 system attains final phenol and TOC conversion of ca. 40 and 30% respectively with a CO_2 selectivity of ca. 10% (Fig. 1E). The $MnCeO_x$ catalyst shows once again a total phenol conversion after ca. 3 h, while the final TOC conversion is equal to 80–85% and the CO_2 selectivity ca. 20% (Fig. 1F). In this case the lack in carbon mass balance is 20 and 60% for Pt/CeO_2 and $MnCeO_x$ systems, respectively (Table 2).

Notably, no significant leaching of Pt and MnO_x active phases was detected throughout the catalytic tests [1,3,5,8–14,19,24,27–30].

4.2. Characterization of the used catalysts and carbon-mass balance

The systematic gap between TOC conversion and CO_2 selectivity signals a lack in carbon mass balance that could depend on the "stripping" of organic species from the reacting solution [1] and/or the accumulation of C-containing species on the catalyst surface [1,3–5,10–14,18–21,24,29]. Probably consequent to the low phenol conversion and mineralization efficiency of the Pt/CeO_2 catalyst (Fig. 1), HPLC and TOC analyses confirmed the presence of phenol, acrylic, acetic and formic acids in the cold trap solution at $R < 5$ [1]. Their cumulative amount corresponds to ca. 10 and 13% of the initial carbon loading (i.e., 6×10^{-2} mol L^{-1}) for R of 2 and 1 respectively, accounting for an almost constant (6–8%) theoretic carbon content of all the used Pt/CeO_2 samples (Table 2). At variance the lack of any TOC in the cold trap solution discloses that the deficit in carbon mass-balance recorded for the $MnCeO_x$ system is always due to the accumulation of carbon deposits on the catalyst surface and, therefore, their amount on the used samples must systematically raise with R (Table 2). Accordingly, the TGA-DSC data in Fig. 2 show that the used Pt/CeO_2 and $MnCeO_x$ catalysts at $R = 5$ feature a weight loss of 6 and 5% respectively, in concomitance with an exothermic DSC peak of comparable intensity (ca. 1 mV/g) relative to the combustion of adsorbed C-species [1,13,14,29]. The $MnCeO_x$ sample shows a fairly symmetric combustion peak spanned in the range of 250–325 °C and centered at

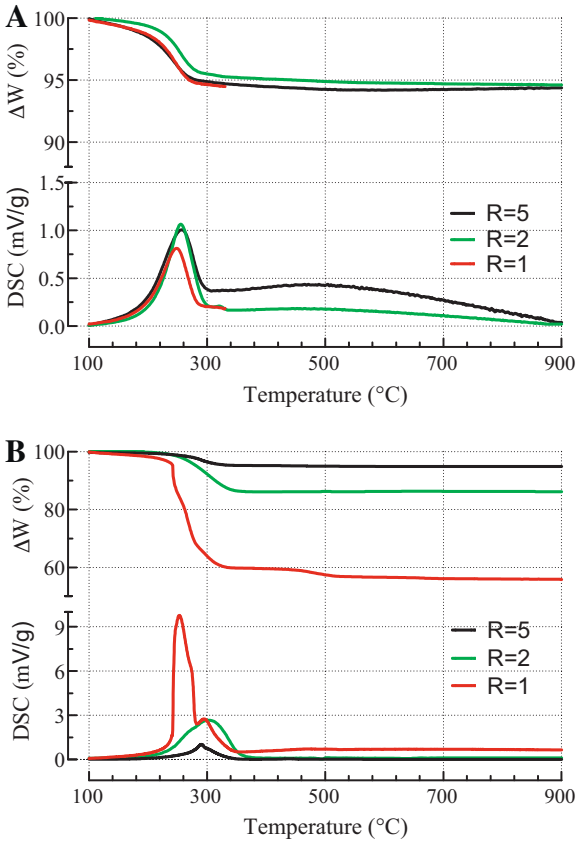

Fig. 2. TGA-DSC data of the used Pt/CeO_2 (A) and $MnCeO_x$ (B) catalysts at different catalyst-to-phenol weight ratio (R).

ca. 290 °C (Fig. 2B), while for the Pt/CeO_2 the DSC peak spans the range of 100–300 °C being centered at ca. 260 °C (Fig. 2A). A further very broad and poorly intense exothermic signal, spanned in the range of 350–900 °C, and corresponding to a minor (≈1%) weight loss, likely monitors the slower oxidation of carbon deposits at the surface of the ceria carrier (see *infra*). The used Pt/CeO_2 and $MnCeO_x$ catalysts at $R = 2$ show a weight loss of ca. 5 and 15% respectively and minor changes in position and shape of the DSC peaks with respect to $R = 5$, though a ca. threefold intensity well accounts for the higher C-content of the latter sample. The used Pt/CeO_2 sample at $R = 1$ features a weight loss still equal to 6%, the relative DSC peak showing no variations in shape and position with reference to previous samples. For the used $MnCeO_x$ sample the weight loss is instead ca. 40% (Fig. 2B), according to the ca. 60% gap between final TOC abatement and CO_2 selectivity values (Table 2). A correspondingly larger DSC peak shows in this case the contribution of an overwhelming component centered at ca. 260 °C convoluted with a smaller peak, comparable for position and intensity with that of used samples at higher R (Fig. 2B), attributable to less reactive adsorbed intermediates [1,5,10–14,18–21,29,30].

All TGA data give a reliable carbon mass-balance (Table 2) confirming the close link between phenol/TOC conversion (Fig. 1) and surface adsorption process [1,3,4,11–14,29].

Then, the changes in the surface chemical composition brought by the reaction medium were probed by a comparative XPS study of the fresh and used catalysts at R of 5 and 1, the data being reported in Table 3. In addition, information on the oxidation state of Pt and Mn phases was obtained from the analysis of the relative XPS spectra (Fig. C of Supplementary information). A surface Pt/Ce atomic ratio (0.1) more than one order of magnitude lower than Mn/Ce one (1.4) in the fresh samples mirrors the chemical

Table 3
XPS data of the "fresh" and "used" catalysts: surface atomic abundance and ratios.

Catalyst	Sample history	Atomic abundance				Atomic ratio	
		Ce	Me[a]	C	O	Me/Ce	C/O[b]
Pt/CeO_2	Fresh	34.7	3.1	–	62.2	0.1	–
	Used, $R=5$	11.3	1.1	46.7	40.9	0.1	2.5
	Used, $R=1$	0.8	0.1	83.3	15.8	0.1	5.9
$MnCeO_x$	Fresh	15.4	21.2	–	63.4	1.4	–
	Used, $R=5$	4.4	8.0	50.4	37.2	1.8	3.1
	Used, $R=1$	0.2	0.7	74.8	24.3	3.5	3.3

[a] Me stands for Pt and Mn, respectively.
[b] Surface C/O atomic ratio corrected from the contribution of oxide lattice oxygen.

characteristics of supported (Pt/CeO_2) and bulk ($MnCeO_x$) catalysts, respectively. Moreover, while the Pt spectrum indicates a prevalent metallic state in the fresh Pt/CeO_2 sample further to the prereduction-passivation treatment (see Section 2), an average oxidation number of ca. +3.4 is obtained for Mn from the main $Mn_{2p3/2}$ peak position (642.2 eV) and $Mn_{2p3/2}$–$Mn_{2p1/2}$ *spin–orbit* split value (11.5 eV) [33–36]. Beside to a considerable decrease of the Pt, Mn and Ce signals intensity due to build-up of carbon deposits on the catalyst surface mostly at $R=1$ (Fig. C of Supplementary information), the reaction system affects also composition and oxidation state of the active phases. An evident growth of the Mn/Ce ratio on the used $MnCeO_x$ catalyst (Table 3) is likely diagnostic of a prevalent coverage of the ceria matrix by carbon species, consistent with the poor mineralization activity under reaction conditions. In addition, while an unchanged peaks position discloses no significant changes in the average Mn oxidation number with reference to fresh $MnCeO_x$ sample, a ca. 2 eV upward shift of the XPS profiles (Fig. C of Supplementary information) is consistent with the oxidation of Pt to PtO [34]. These findings prove the efficiency of the reaction setup in enabling a constant oxygen supply to the catalyst surface, driving the heterogeneous oxidation path at the adopted conditions of oxygen flow, pressure and stirring rate [1]. Furthermore, according to testing and TGA-DSC results, the used samples present an overwhelming surface concentration of carbon and oxygen atoms, the relative concentration of which provides a measure of their oxidative pattern. In particular, an unchanging O/C atomic ratio of ca. 3 (Table 3) signals an oxidative strength of the $MnCeO_x$ sample independent from R due to a uniform active sites distribution across the catalyst surface. While, a O/C ratio rising from 2.5 ($R=5$) to 6 ($R=1$) suggests that the Pt/CeO_2 system explicates a better mineralization activity at low surface phenol loadings because of the poorer exposure of active Pt sites (see *infra*).

4.3. Mechanistic-kinetic analysis of the CWAO pattern

Although efficiency, mechanism and kinetics of heterogeneous and homogeneous CWAO are still matter of debate [1,3–6,11–27,30,31], current experimental findings substantiate the fundamental role of surface adsorption on the working mechanism of both Pt/CeO_2 and $MnCeO_x$ catalysts [1,3,11–14,18,29,37]. Indeed, just the adsorption explains the "optimal" water purification efficiency of the heterogeneous systems, fixed by the straight-line relationship between phenol and TOC conversion (Fig. 3). The simultaneous abatement (*conversion*) of phenol and TOC is in fact diagnostic of an "ideal" selective CWAO pattern (Fig. 3) leading to the degradation of the substrate to CO_2 (*mineralization*) without residual intermediates formation [1,3,11–14,18–20,29,37]. At variance, the exponential-rising trends (Fig. 3) depicted by homogeneous Cu^{2+}, Fe^{3+} and Mn^{2+} catalysts [1] stress the basic role of "unsaturated" reaction intermediates on the radical-chain propagation leading to the ultimate formation of CO_2 and, mostly, of C1–C2 acids [1,8,9,15,20,30,37]. Then,

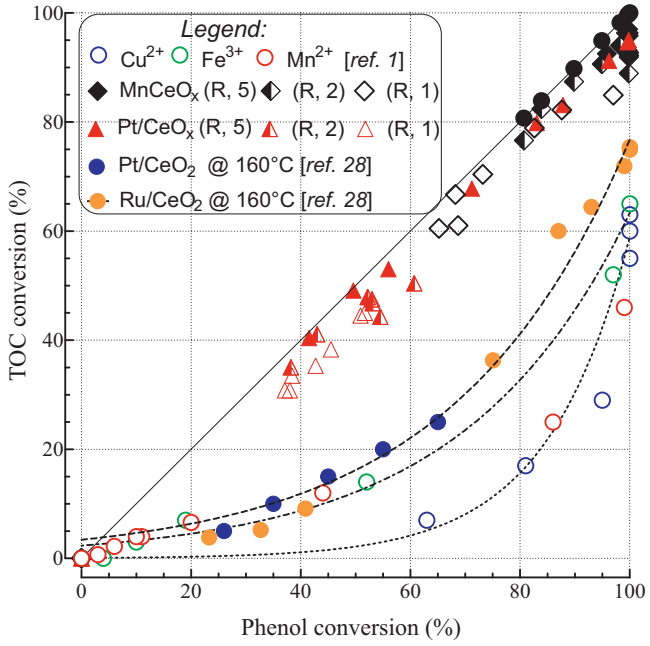

Fig. 3. Comparison of the CWAO pattern of Pt/CeO_2 and $MnCeO_x$ catalysts at various catalyst-to-phenol weight ratio (R) with that of homogeneous systems [1]: TOC *vs.* phenol conversion. Data of Pt/CeO_2 and Ru/CeO_2 @ 160 °C taken from [28] for comparison.

the fact that reference literature data of CeO_2-based noble-metals (Pt and Ru) [28] match with the trend of homogeneous CWAO (Fig. 4) discloses the prevalent occurrence of the radical path as consequence of the different experimental conditions and setup [27,28,30]. Indeed, those data were obtained under a static oxygen atmosphere and they likely reflect the less effective oxygen supply to the catalyst surface [28]. This hinders the surface oxidation path, leading to a consequent release of C4–C6 intermediates that enable the free-radical reaction network [28,30], as substantiated by the analogous "phenol-TOC" conversion relationships found in trickle-bed and slurry reactors respectively [9], as a consequence of a different interphase oxygen transfer efficiency [5,9].

Therefore, the catalytic pattern of the studied catalysts is describable by a dual-site Langmuir–Hinshelwood (L–H) path [1,3,10–14,29,37] involving consecutive phenol adsorption (conversion) and mineralization (CO_2 formation) steps on "α" and "σ—O" surface sites respectively (see Scheme 1). By-product release/desorption and carbon deposition are the undesired side-reactions proceeding in parallel to the mineralization step and accounting for residual TOC (Fig. 1) and catalyst fouling (Fig. 2), respectively. Considering that α represents a generic adsorption site, σ—O and σ the active oxidation sites in the oxidized and reduced form respectively, while P is a generic partial oxidation intermediate, the catalytic loop involves the

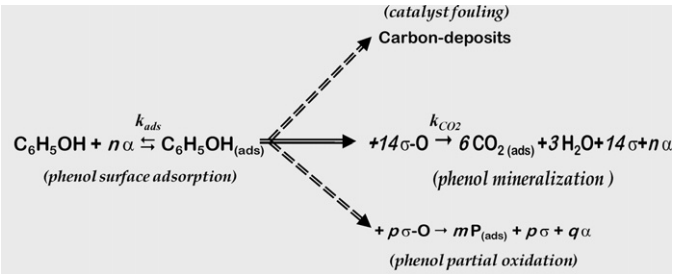

Scheme 1. Simplified reaction scheme of the heterogeneous CWAO of phenol.

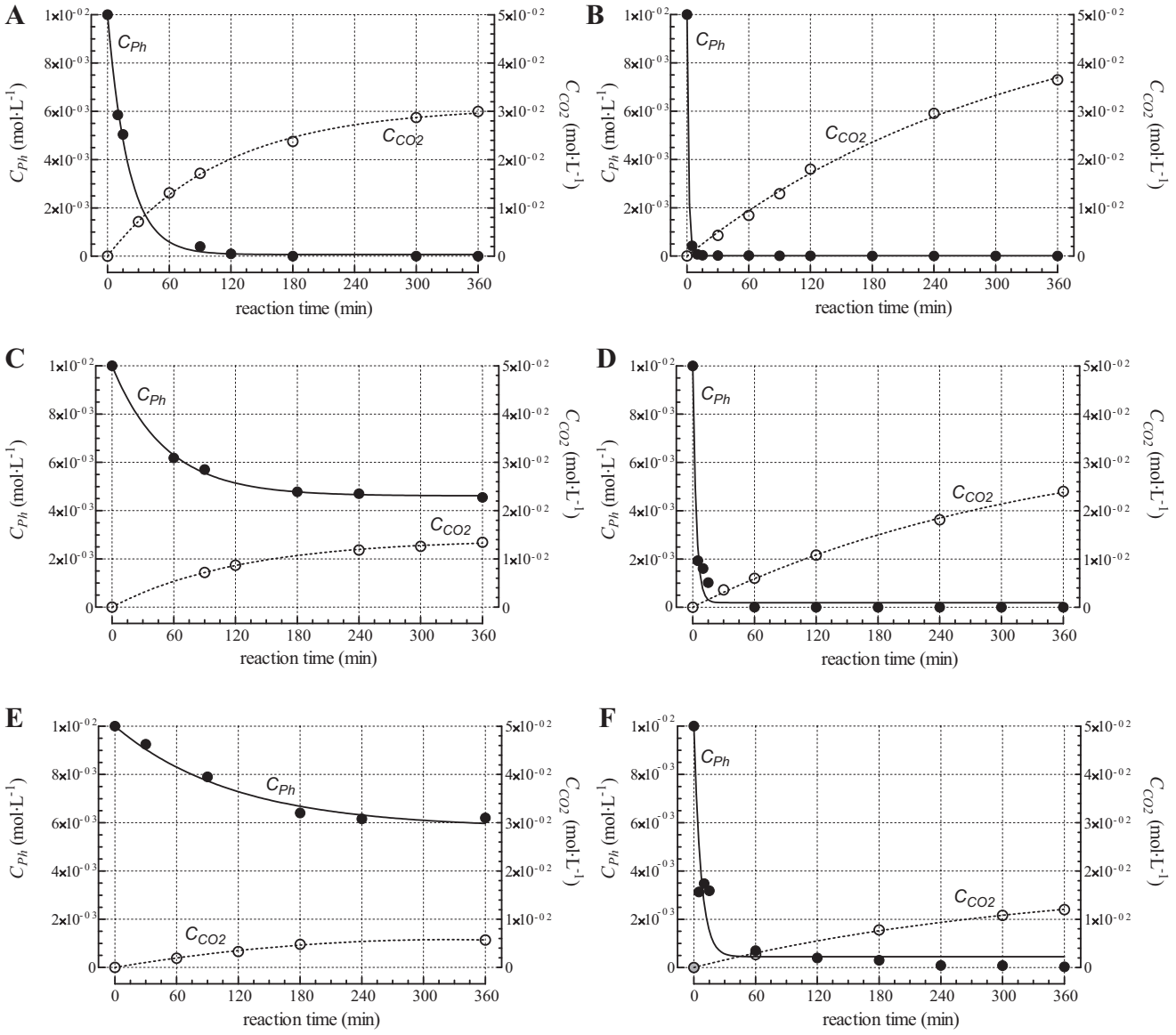

Fig. 4. 1st-order kinetic fit (solid lines) by Eq. (4) of phenol concentration (C_{Ph}, ●) and CO_2 concentration (CO_2, ○) experimental data of Pt/CeO_2 (A, C, E) and $MnCeO_x$ (B, D, F) catalysts at catalyst-to-phenol weight ratio (R) of 5 (A and B), 2 (C and D) and 1 (E and F).

re-oxidation of reduced sites σ formed by oxidation of adsorbed species (a) and the CO_2 (b) and intermediate (c) desorption, with replenishing of a corresponding number of α adsorption sites:

(a)	$\sigma + 1/2O_2 \rightarrow \sigma\text{—}O$	(active site re-oxidation)
(b)	$CO_{2(ads)} \leftrightarrows CO_2\uparrow + m\alpha$	(CO_2 desorption)
(c)	$P_{(ads)} \rightarrow P\uparrow + q\alpha$	(intermediate desorption)

For the sake of simplicity, the re-adsorption and further oxidation of intermediates to CO_2 are neglected as P mostly consists of the refractory acetic acid, the concentration of which rises in fact throughout reaction time, according to the regular decrease of pH at any conditions (Fig. 1). The above scheme satisfies the following evidences:

- the surface oxidation of phenol, leading to CO_2 formation (C-mineralization), is slower in comparison to adsorption and re-oxidation of active sites (a);
- the CO_2 desorption (b) is fast and irreversible owing to the acidic pH (3–4), favoring its displacement in the gas-phase;
- the effects of the parallel steps leading to intermediates and carbon-deposits on the initial rates of phenol adsorption and CO_2 formation are negligible as they proceed with a comparatively slower rate.

Although the nature of adsorption sites (α) is still undefined, being somewhat related to catalyst texture [1,11–14,29], their concentration does not depend only on surface area and pore volume that are comparable for the two systems (Table 1). Then, the rate of phenol (undissociative) adsorption can be formally expressed by a pseudo 1st-order kinetic model:

$$\text{rate}_{Ph} = -\frac{dC_{Ph}}{dt} = k_{Ph}(C_{Ph} - C_{Ph,fin}) \quad (3)$$

where C_{Ph} is the phenol concentration at time t and $C_{Ph,fin}$ is the final concentration (t, 6 h). However, due to the high levels of phenol conversion (Fig. 1), the integral form of the 1st-order model between initial and final concentration ($C_{Ph,fin}$):

$$\frac{C_{Ph} - C_{Ph,fin}}{C_{Ph,in} - C_{Ph,fin}} = e^{-k_{Ph}t} \quad (4)$$

was used to fit the experimental phenol concentration (C_{Ph}) data, as shown in Fig. 4. Eq. (4) fitting curve allows obtaining the

Table 4
Data summary of the pseudo 1st-order kinetic fit of phenol conversion (Eq. (4)) and CO_2 formation (Eq. (8)) at various catalyst-to-phenol weight ratio (R).

Catalyst	$C_{Ph,in}$ (mol L^{-1})	C_{cat} (g/L)	R (w_{cat}/w_{Ph})	$C_{Ph,fin}$ (mol L^{-1})	$C_{Ph,ads}$[a] (g_{Ph} g_{cat}^{-1})	k_{Ph} (h^{-1})	r^2	$rate_{Ph}$[b] (mol_{Ph} L^{-1} h^{-1})	k_{CO_2}	r^2 (h^{-1})
Pt/CeO_2	1.0×10^{-2}	5	5	$0.0\times10^{+0}$	0.20	$3.0\times10^{+0}$	0.97	3.0×10^{-2}	6.6×10^{-1}	1.00
	1.0×10^{-2}	2	2	4.4×10^{-3}	0.28	$1.2\times10^{+0}$	1.00	1.2×10^{-2}	3.0×10^{-1}	1.00
	1.0×10^{-2}	1	1	6.1×10^{-3}	0.39	5.1×10^{-1}	0.98	5.1×10^{-3}	1.2×10^{-1}	1.00
$MnCeO_2$	1.0×10^{-2}	5	5	$0.0\times10^{+0}$	0.20	$3.8\times10^{+1}$	1.00	3.8×10^{-1}	8.8×10^{-1}	1.00
	5.0×10^{-2}	25	5[c]	$0.0\times10^{+0}$	0.20	$3.7\times10^{+1}$	1.00	$1.9\times10^{+0}$	$1.1\times10^{+0}$	1.00
	1.0×10^{-2}	2	2	$0.0\times10^{+0}$	0.50	$1.8\times10^{+1}$	0.99	1.8×10^{-1}	4.6×10^{-1}	1.00
	1.0×10^{-2}	1	1	$0.0\times10^{+0}$	1.00	$8.9\times10^{+0}$	0.97	8.9×10^{-2}	2.2×10^{-1}	1.00

[a] Amount of phenol adsorbed at $t = 6$ h.
[b] Initial phenol conversion rate data obtained as the product of the decay constant k_{Ph} (Fig. 4) by the initial phenol concentration ($C_{Ph,in} = 0.01$ mol L^{-1}).
[c] Data obtained at $R = 5$ using fivefold concentration of both phenol and catalyst (Fig. B of Supplementary information).

1st-order decay constants (k_{Ph}, h^{-1}) and the initial phenol conversion rates ($rate_{Ph}$, mol_{Ph} L^{-1} h^{-1}) as the product of k_{Ph} by the initial phenol concentration ($C_{Ph,in}$, 0.01 mol L^{-1}), summarized in Table 4. The reliable data fitting ($r^2 > 0.97$) by Eq. (4) discloses k_{Ph} values (9–38 h^{-1}) for the $MnCeO_x$ catalyst systematically larger by more than one order of magnitude than those of Pt/CeO_2 (k_{Ph}, 0.5–3.0 h^{-1}), in both cases raising regularly with R. Due to the unchanging initial phenol concentration (0.01 mol L^{-1}), the conversion rate keeps the same trend of k_{Ph}, while fivefold concentrations of both phenol (5 g/L) and catalyst (25 g/L) give the same k_{Ph} value found at $R = 5$ and a five times higher $rate_{Ph}$ (Table 4).

Although selectivity data in Fig. 1 are determined from to the amount of CO_2 stripped away from the reacting solution by the oxygen flow and trapped in the $Ba(OH)_2$ solution, for comparative purposes these have been transformed in concentration data referred to the reacting solution (C_{CO_2}, mol L^{-1}), as shown in Fig. 4. According to the reaction scheme (1), and considering that the continuous feed ensures an overwhelming concentration of oxygen in the reacting solution, the CO_2 formation or C-mineralization rate (mol_{CO_2} L^{-1} h^{-1}) is (pseudo) 1st-order with respect to the amount of adsorbed phenol $C_{Ph,ads}$ (mol g_{cat}^{-1}):

$$rate_{CO_2} = \frac{dC_{CO_2}}{dt} = -\frac{dC_{Ph,ads}}{dt}C_{cat} = (k'_{CO_2}C_{O_2})C_{Ph,ads}C_{cat} = k_{CO_2}C_{Ph,ads}C_{cat} \quad (5)$$

with $k_{CO_2} = (k'_{CO_2}C_{O_2})$ being the apparent kinetic constant of CO_2 formation. Considering the following relationship between phenol concentration in the solution and amount adsorbed on the catalyst:

$$(C_{Ph,in} - C_{Ph}) = C_{Ph,ads}C_{cat} \quad (6)$$

the rate of CO_2 formation can be rewritten as

$$rate_{CO_2} = \frac{dC_{CO_2}}{dt} = k_{CO_2}(C_{Ph,in} - C_{Ph}) \quad (7)$$

showing that the apparent kinetic constant of CO_2 formation corresponds to the slope of the derivative function

$$\frac{dC_{CO_2}}{(C_{Ph,in} - C_{Ph})} = k_{CO_2}dt \quad (8)$$

With a theoretic limit of 6 corresponding to the maximum number of CO_2 molecules per molecule of phenol (i.e., $S_{CO_2} = 100\%$), during the first 3 h that function results in all the cases in fairly accurate straight-line relationships (Fig. 5) that are diagnostic of a constant mineralization rate of the adsorbed substrate. Afterward a decline of the slope, more evident for the Pt/CeO_2 catalyst (Fig. 5), discloses a systematic slowing down of the mineralization process accounting for a harder mineralization of the residual adsorbed substrate, favoring the formation/release of partial oxidation intermediates and catalyst fouling (Scheme 1). The slope of the above linear relationships (k_{CO_2}, h^{-1}) provides the values

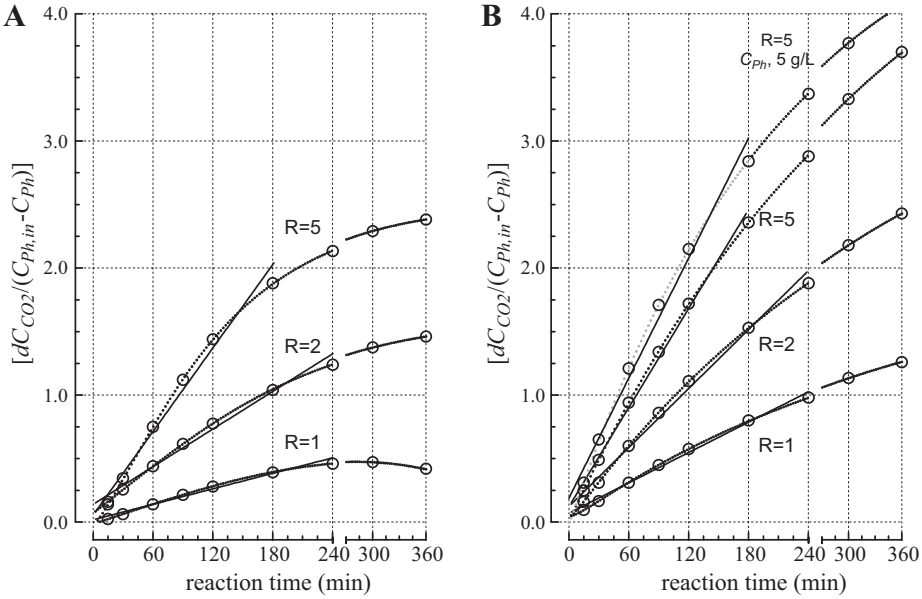

Fig. 5. Plot of the "$dC_{CO_2}/(C_{Ph,in} - C_{Ph})$" derivative function (Eq. (8)) *vs.* reaction time of Pt/CeO_2 (A) and $MnCeO_x$ (B) catalysts at catalyst-to-phenol weight ratio (R) of 5, 2 and 1 (Fig. 4).

of the pseudo 1st-order kinetic constant of CO_2 formation, listed in Table 4. In agreement with XPS data (Table 3), the $MnCeO_x$ system ensures a faster mineralization of the substrate at any R, according to k_{CO_2} values (2.2×10^{-1} to 9.5×10^{-1} h^{-1}) ca. two times greater than Pt/CeO_2 catalyst (1.2×10^{-1} to 6.6×10^{-1} h^{-1}). In addition, although rising with R, a fivefold larger concentration of both phenol and catalyst at $R = 5$ has not effects on k_{CO_2} value (Table 4).

The systematic trends in k_{Ph} and k_{CO_2} with R (Table 4) reveal that catalyst concentration (C_{cat}, g/L) determines the overall reaction kinetics, as confirmed by the log-plot of k_{Ph} and k_{CO_2} *vs.* C_{cat}, in Fig. 6A. Indeed, both k_{Ph} and k_{CO_2} relationships feature a linear dependence on C_{cat} (i.e., $\propto C_{cat}^{0.9-1.1}$), which means unchanging values of the specific pseudo 1st-order catalytic constant ($L\,g_{cat}^{-1}\,h^{-1}$) of both phenol adsorption (k_{ads}, k_{Ph}/C_{cat}) and mineralization (k_{ox}, k_{CO_2}/C_{cat}) steps, as shown in Fig. 6B. In particular, the $MnCeO_x$ catalyst features a k_{ads} value (8.2 ± 0.7 $L\,g_{cat}^{-1}\,h^{-1}$) more than one order of magnitude larger than Pt/CeO_2 (0.5 ± 0.1 $L\,g_{cat}^{-1}\,h^{-1}$), though the kinetic constant of CO_2 formation (k_{ox}, 0.2 ± 0.02 $L\,g_{cat}^{-1}\,h^{-1}$) is only ca. two times higher (k_{ox}, 0.12 ± 0.01 $L\,g_{cat}^{-1}\,h^{-1}$). Therefore, a k_{ox} much smaller than k_{ads} ($k_{ads}/k_{ox} \approx 40$) confirms that the mineralization is the rate limiting step (r.l.s.) of phenol CWAO on $MnCeO_x$ catalysts [1,10–14,29,37], while adsorption and mineralization steps proceed with a comparable rate on the Pt/CeO_2 system ($k_{ads}/k_{ox} \approx 4$).

The functionality of the two systems is further compared in Fig. 6C in terms of initial phenol specific surface adsorption rate (SSA_{ads}, $mol_{Ph}\,m_{cat}^{-2}\,h^{-1}$) and surface adsorption capacity (SAC, $g_{Ph}\,m_{cat}^{-2}$). Because of their comparable surface area (Table 1), the superior purification efficiency of the $MnCeO_x$ catalyst emerges from a SSA_{ads} value ($1.0 \pm 0.1 \times 10^{-3}$ $mol_{Ph}\,m_{cat}^{-2}\,h^{-1}$) more than one order of magnitude larger than that of Pt/CeO_2 ($6.5 \pm 0.5 \times 10^{-5}$ $mol_{Ph}\,m_{cat}^{-2}\,h^{-1}$). In addition the $MnCeO_x$ system features a phenol surface adsorption capacity of 1.2×10^{-2} $g_{Ph}\,m_{cat}^{-2}$, well accounting for a weight loss greater than 40% of the used sample at $R = 1$ (Fig. 2), in comparison to a value of $3–4 \times 10^{-3}$ $g_{Ph}\,m_{cat}^{-2}$ of the Pt/CeO_2 system (Fig. 6C). This weaker surface affinity of the Pt/CeO_2 system to phenol should mirror the prevailing surface exposure of the poorly reactive ceria carrier [8,19,24,28], according to a MSA/SA ratio of 3% (Table 1) and a $Pt_{at}/Ce_{at} \approx 0.1$ (Table 3). Whereas, favoring a prevailing exposure of the active phase (Table 3), the high MnO_x loading promotes the CWAO performance of the $MnCeO_x$ system in terms of both adsorption rate and capacity (≥ 1.0 g_{Ph}/g_{cat}). However, considering the fairly different loading of active phase (Table 1), the normalization of both adsorption (k'_{ads}) and mineralization (k'_{ox}) kinetic constants to the metal loading ($L\,g_{Me}^{-1}\,h^{-1}$) allows getting insights into the intrinsic CWAO functionality of Pt and MnO_x active phases. In fact a k'_{ads} of ca. 31 ± 3 $L\,g_{Mn}^{-1}\,h^{-1}$, ca. 3 times larger than that of the Pt/CeO_2 system (10 ± 2 $L\,g_{Pt}^{-1}\,h^{-1}$), suggests that the better phenol adsorption functionality of the $MnCeO_x$ system depends also upon a higher surface affinity of the active phase to phenol. Whereas, a k'_{ox} (2.4 ± 0.2 $L\,g_{Pt}^{-1}\,h^{-1}$) ca. three times larger than that of the $MnCeO_x$ catalyst (0.75 ± 0.08 $L\,g_{Mn}^{-1}\,h^{-1}$) substantiates the stronger oxidation activity of the active Pt phase. Despite the quite larger SROA (Table 1) linked to the well known promoting effect of Pt on the oxygen-mobility of underlying ceria matrix [27,28,30,38], yet the smaller k_{ox} value of the Pt/CeO_2 system (Table 4) substantiates further the scarce efficiency of ceria carrier in driving the phenol mineralization process [3–5,19,27,28]. Then, such different rates and capacities of phenol adsorption and mineralization should influence the resistance to deactivation by fouling of the studied catalysts, as confirmed by forthcoming stability tests results.

D) Stability tests and deactivation pattern. In the light of the above reaction network, the surface oxidation step controls at once the

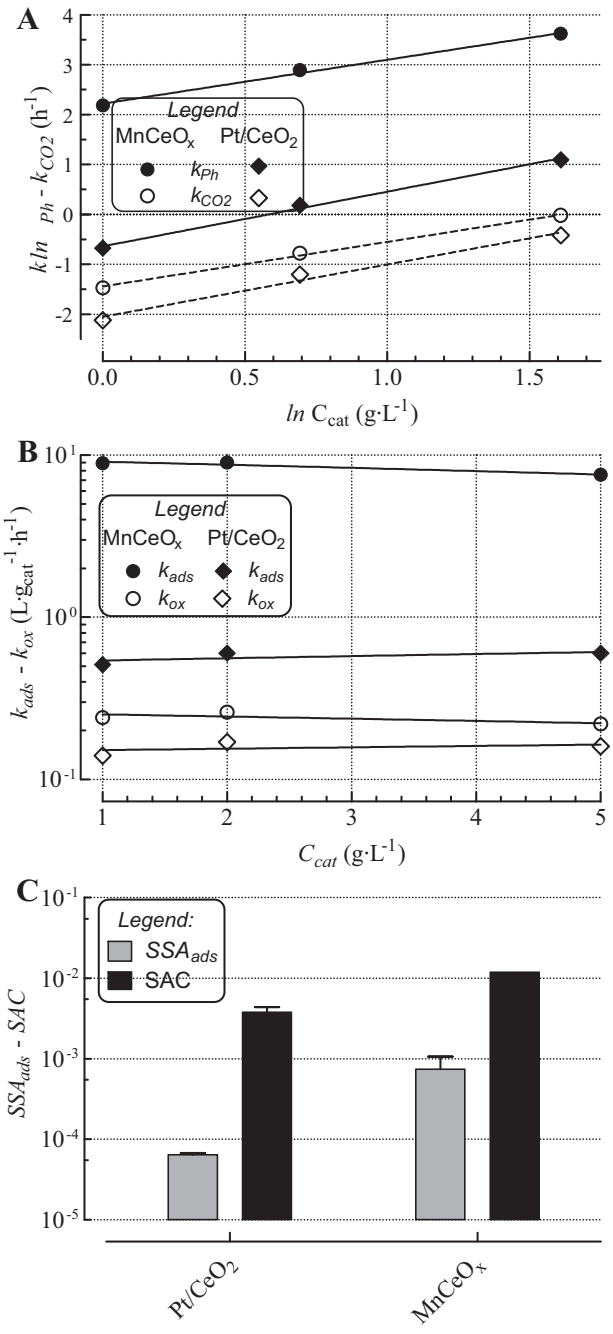

Fig. 6. (A) "Log-plot" of the rate of the kinetic constant of phenol concentration decay (k_{Ph}, ● and ♦) and CO_2 formation (k_{CO_2}, ○ and ◊) *vs.* catalyst concentration (C_{cat}, g/L); (B) effect of the catalyst concentration on the catalytic kinetic constant of phenol adsorption (k_{ads}, ● and ♦) and CO_2 formation (k_{ox}, ○ and ◊); (C) initial specific surface rate of phenol adsorption (SSA_{ads}, $mol_{Ph}\,m_{cat}^{-2}\,h^{-1}$) and surface adsorption capacity (SAC, $g_{Ph}\,m_{cat}^{-2}$) of Pt/CeO_2 and $MnCeO_x$ catalysts.

by-product selectivity and the build up of carbonaceous deposits and, in turn, the catalyst stability [9–14,18–21,24,28,29]. To get information on the resistance to deactivation, which constitutes the most critical issue of heterogeneous CWAO systems [2–5], comparative stability tests were carried out running five consecutive reaction cycles of 6 h at a constant R of 5. The results are shown in Fig. 7 in terms of phenol and TOC conversion (A and B), CO_2 selectivity (C and D) and trends of k_{ads} and k_{ox} during five reaction cycles (E and F). The poorer CWAO efficiency of the Pt/CeO_2 system is confirmed by a continuous decay of the extent of phenol removal

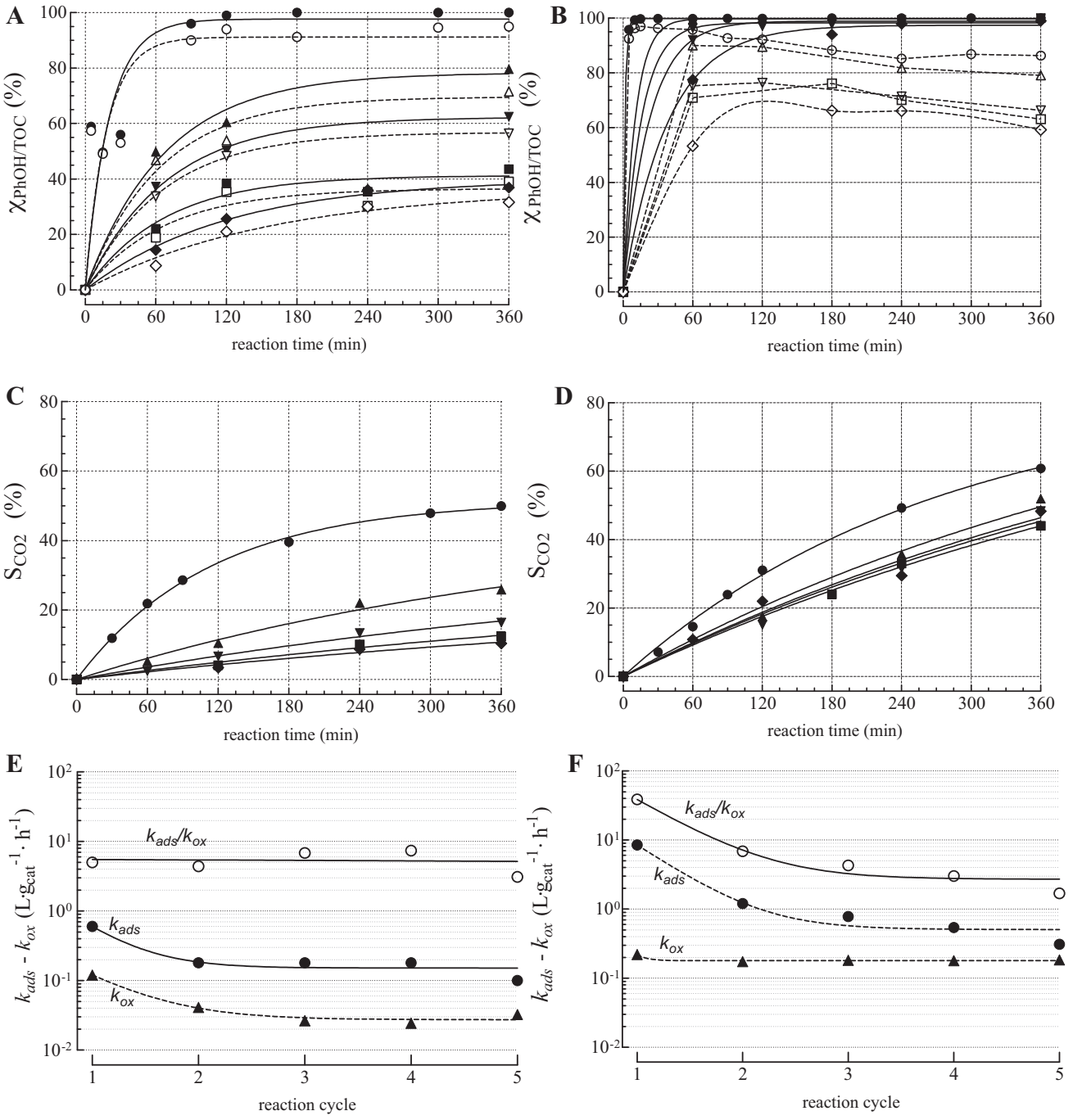

Fig. 7. Stability test of the Pt/CeO_2 (A, C, E) and $MnCeO_x$ (B, D, F) catalysts in the CWAO of phenol at 150 °C during 5 reaction cycles at $R = 5$: phenol (full symbols) and TOC (open symbols) conversion *vs.* reaction time (A and B); CO_2 selectivity *vs.* reaction time (C and D); pseudo 1st-order kinetic constant of phenol adsorption (k_{ads}, ●) and CO_2 formation (k_{ox}, ▲) and their ratio (k_{ads}/k_{ox}) during five reaction cycles (E and F).

from 100 to 40% (Fig. 7A), corresponding to a lowering of k_{ads} from 6×10^{-1} to ca. 1×10^{-1} L g_{cat}^{-1} h^{-1} (Fig. 7E). On the whole these data correspond to an adsorption capacity of 0.60 g_{Ph}/g_{cat}, which is larger than the value of 0.3–0.4 g_{Ph}/g_{cat} previously found at $R < 5$. This could be due to the foreseen more effective mineralization of the adsorbed substrate at lower surface loadings, enhancing the adsorption of the substrate in subsequent cycles. Indeed, despite the CO_2 selectivity falls from ca. 50 to 10% (Fig. 7C), mirroring a decay of k_{ox} from 1.2×10^{-1} to 3×10^{-2} L g_{cat}^{-1} h^{-1} (Fig. 7E), a cumulative phenol mineralization capacity of ca. 0.25 g_{Ph}/g_{cat} well exceeds the value of ca. 0.1 g_{Ph}/g_{cat} recorded at $R < 5$ (Fig. 1).

The $MnCeO_x$ features an evidently superior resistance to deactivation ensuring a full phenol removal throughout all reaction cycles (Fig. 7B), in agreement with the adsorption capacity of 1.0 g_{Ph}/g_{cat} previously found at R of 1 (Fig. 6C). Although k_{ads} lowers from 8.5 to 6×10^{-1} L g_{cat}^{-1} h^{-1} (Fig. 7F) it should be noticed that the last value is still comparable with that of the fresh Pt/CeO_2 system (Fig. 7E). The CO_2 selectivity decreases slightly during the five reaction cycles (Fig. 7D), according to an almost constant k_{ox} (Fig. 7F) ensuring an overall mineralization capacity of ca. 0.5 g_{Ph}/g_{cat} that, also in this case, is markedly larger than that found (≈0.2 g_{Ph}/g_{cat}) at $R < 5$ (Fig. 1). These data confirm that also the stability pattern

depends upon the different structural features of the studied catalysts. Indeed, the comparable decay of k_{ads} and k_{ox} (Fig. 7E) is consistent with the fact that both adsorption and mineralization functionalities are mostly associated with the Pt phase, while slight, if any, is the contribution of the ceria support to the reactivity pattern of the Pt/CeO_2 catalyst [5,18–21,27,28,30]. Whereas, matching the *dual-site* nature of the reaction path, the deep decay of the adsorption functionality (Fig. 7F) signals a stronger impact of fouling by carbonaceous deposits on the surface exposure and adsorption sites availability [1,11–14,29], at variance of the mineralization functionality depending mostly on the redox properties of the active phase [1,11–14,29].

5. Conclusions

The performance of noble-metal (Pt/CeO_2) and transition metal-oxide ($MnCeO_x$) catalysts in the wet air oxidation of phenol (CWAO) at 150 °C has been systematically probed in terms of activity, selectivity and resistance to deactivation by fouling.

A simplified Langmuir–Hinshelwood (L–H) reaction network based on consecutive phenol *adsorption* and *mineralization* steps explains the reactivity pattern of Pt/CeO_2 and $MnCeO_x$ catalysts and their CWAO superior efficiency with respect to homogeneous systems.

The $MnCeO_x$ system shows a better CWAO performance in terms of phenol adsorption rate ($\approx 8\ g_{Ph}\ g_{cat}^{-1}\ h^{-1}$), capacity ($>1\ g_{Ph}/g_{cat}$) and mineralization ($>0.5\ g_{Ph}/g_{cat}$), conferring also a higher resistance to deactivation by *fouling* than Pt/CeO_2.

The superior CWAO pattern of the $MnCeO_x$ system relies on higher surface affinity to phenol and availability of total oxidation sites due to the high loading and surface exposure of the active phase.

Appendix A. Supplementary data

Supplementary data associated with this article can be found, in the online version, at doi:10.1016/j.apcatb.2011.12.035.

References

[1] F. Arena, C. Italiano, A. Raneri, C. Saja, Appl. Catal. B 99 (2010) 321–328.
[2] G. Busca, S. Berardinelli, C. Resini, L. Arrighi, J. Hazard. Mater. 160 (2008) 265–288.
[3] K.H. Kim, S.-K. Ihm, J. Hazard. Mater. 186 (2011) 16–34.
[4] S.K. Bhargava, J. Tardio, J. Prasad, K. Foger, D.B. Akolekar, S.C. Grocott, Ind. Eng. Chem. Res. 45 (2006) 1221–1258.
[5] F. Larachi, Top. Catal. 33 (2005) 109–134.
[6] S.T. Kolaczkowski, P. Plucinski, F.J. Beltran, F.J. Rivas, D.B. McLurgh, Chem. Eng. J. 73 (1999) 143–160.
[7] J. Kemsley, Chem. Eng. News 86 (2008) 71–73.
[8] S. Imamura, Ind. Eng. Chem. Res. 38 (1999) 1743–1753.
[9] Y.I. Matatov-Meytal, M. Sheintuch, Ind. Eng. Chem. Res. 37 (1998) 309–326.
[10] S.T. Hussain, A. Sayari, F. Larachi, J. Catal. 201 (2001) 153–157.
[11] M. Abecassis-Wolfovich, M.V. Landau, A. Brenner, M. Herskowitz, Ind. Eng. Chem. Res. 43 (2004) 5089–5097.
[12] M. Abecassis-Wolfovich, R. Jothiramalingam, M.V. Landau, M. Herrskowitz, B. Viswanathan, T.K. Varadarajan, Appl. Catal. B 59 (2005) 91–98.
[13] F. Arena, J. Negro, G. Trunfio, A. Parmaliana, Ind. Eng. Chem. Res. 46 (2007) 6724–6731.
[14] F. Arena, G. Trunfio, J. Negro, L. Spadaro, Appl. Catal. B 85 (2008) 40–47.
[15] S. Hočevar, J. Batista, J. Levec, J. Catal. 184 (1999) 39–48.
[16] F. Arena, R. Giovenco, T. Torre, A. Venuto, A. Parmaliana, Appl. Catal. B 45 (2003) 51–62.
[17] F. Arena, E. Alongi, P. Famulari, A. Parmaliana, G. Trunfio, Catal. Lett. 107 (2006) 39–46.
[18] A. Santos, P. Yustos, A. Quintanilla, G. Ruiz, F. García-Ochoa, Appl. Catal. B 61 (2005) 323–333.
[19] S.-K. Kim, S.-K. Ihm, Top. Catal. 33 (2005) 171–179.
[20] A. Quintanilla, J. Casas, A.F. Mohedano, J.J. Rodriguez, Appl. Catal. B 67 (2006) 206–216.
[21] R. Kouraichi, J.J. Delgado, J.D. López-Castro, M. Stitou, J.M. Rodríguez-Izquierdo, M.A. Cauqui, Catal. Today 154 (2010) 195–201.
[22] Q. Wu, X. Hu, P.-l. Yue, Chem. Eng. Sci. 58 (2003) 923–928.
[23] J. Pintar, J. Levec, J. Catal. 135 (1992) 345–357.
[24] H. Chen, A. Sayari, A. Adnot, F. Larachi, Appl. Catal. B 32 (2001) 195–204.
[25] J. Vicente, R. Rosal, M. Diaz, Ind. Eng. Chem. Res. 41 (2002) 46–51.
[26] H.R. Devlin, J.J. Harris, Ind. Eng. Chem. Fundam. 23 (1984) 387–392.
[27] D. Duprez, F. Delanoë, J. Barbier, P. Isnard, G. Blanchard, Catal. Today 29 (1996) 317–322.
[28] J. Barbier Jr., L. Oliviero, B. Renard, D. Duprez, Top. Catal. 33 (2005) 77–86.
[29] F. Arena, A. Parmaliana, G. Trunfio, Stud. Surf. Sci. Catal. 172 (2006) 489–492.
[30] S. Nousir, S. Keav, J. Barbier jr., M. Bensitel, R. Brahmi, D. Duprez, Appl. Catal. B 84 (2008) 723–731.
[31] F.J. Rivas, S.T. Kolaczkowski, F.J. Beltran, D.B. McLurgh, Chem. Eng. Sci. 53 (1998) 2575–2586.
[32] H. Zou, Y.S. Lin, N. Rane, T. He, Ind. Eng. Chem. Res. 43 (2004) 3019–3025.
[33] F. Arena, G. Trunfio, J. Negro, B. Fazio, L. Spadaro, J. Phys. Chem. C 113 (2009) 2822–2829.
[34] J.F. Moulder, W.F. Stickle, P.E. Sobol, K.D. Bomben, Handbook of X-ray Photoelectron Spectroscopy, Physical Electronics Inc., Eden Prairie, MN, 1995.
[35] J.C. Carver, G.K. Schweitzer, T.A. Carlson, J. Chem. Phys. 57 (1972) 973–982.
[36] M. Oku, K. Hirokawa, S. Ikeda, J. Electron. Spectrosc. 7 (1975) 465–473.
[37] F. Arena, C. Italiano, A. Raneri, C. Saja, In: M. Theophanides, T. Theophanides (Eds.), Environmental Engineering and Sustainability, Athens, 2010, pp. 297–308.
[38] P. Bera, A. Gayen, M.S. Hegdé, N.P. Lalla, L. Spadaro, F. Frusteri, F. Arena, J. Phys. Chem. B 107 (2003) 6122–6130.